Solid State Ionics 21 (1986) 83–94
North-Holland, Amsterdam

STUDY OF THE OXYGEN ELECTRODE REACTION USING MIXED CONDUCTING OXIDE SURFACE LAYERS. PART II: SMALL SIGNAL ANALYSIS

M.P. VAN DIJK *, K.J. DE VRIES # and A.J. BURGGRAAF
Twente University of Technology, Department of Chemical Engineering, Laboratory for Inorganic Materials Science, P.O. Box 217, 7500 AE Enschede, The Netherlands

Received 23 December 1985; accepted for publication 6 March 1986

The oxygen gas electrode has been studied for a number of mixed conducting oxide surface layers on top of $Gd_2Zr_2O_7$ (TGZO) solid electrolytes. In part II of this paper we present the results of frequency dispersion measurements for the electrode reaction, supplying additional information to the results of current-overvoltage experiments presented in part I. For both kinds of experiments the same trends were observed for the electrode polarization. Best results are obtained for a surface layer of TGZO, while p-type mixed conducting oxides give less decreased values of the electrode polarization. High electrode capacitances were found in the case of mixed conducting surface layers (about 700 F/m^2). The electrode reactions follow a Butler-Volmer type of equation. Most probably a diffusion process is rate controlling the overall charge transfer process.

1. INTRODUCTION

In Part I of this paper we presented the preparation and characterization of layers of mixed conducting oxides on solid electrolytes prepared by radio frequency sputtering. Materials used were the solid electrolyte $Gd_2Zr_2O_7$ (TGZO) and the mixed conducting oxides $Tb_2Zr_2O_{7+y}$ (TGZ100) and $Ce_{0.7}Tb_{0.3}O_{2-y}$ (CT30). Carrying out current-overvoltage experiments for the oxygen gas electrode reaction, it was determined that the presence and nature of a sputtered layer on top of a solid electrolyte has a large effect on the polarization behaviour. With a sputtered layer of the ionic conducting TGZO material the highest current densities were obtained compared to the current densities for the bare solid electrolyte at the same overvoltage values. Mixed, p-type, conducting TGZ100 and CT30 surface layers gave a smaller increase of the current densities. In addition to the current-overvoltage experiments the electrode surface layers are characterized in this part of the paper by small signal complex impedance analysis, yielding information about the electrode resistance (R_{el}):

$$R_{el} = \left(\frac{\eta}{i}\right)_{\eta=0} = \frac{RT}{(\alpha_a+\alpha_c)Fi_0} \qquad [1],$$

and the capacitive behaviour of the electrode interface. Results of the frequency dispersion measurements, according to the experimental procedure outlined in part I of this paper, are split up in a resistive part and a capacitive part for convenience.

* present address: Koninklijke Shell Laboratorium Amsterdam, P.O. Box 3003, 1003 AA Amsterdam, The Netherlands
# to whom correspondence is to be sent

2. RESULTS

2.1 Resistive part

Values of the electrode resistance (R_{el}) were obtained from the complex impedance diagrams as the difference of the intercept values of the polarization curve with the real axis at low and high frequencies.

Fig. 1 shows the electrode resistances as a function of temperature at P_{O_2}=0.21 atm (scaled values according the procedure described in the appendix of part I). Activation enthalpies are listed in Table I. Just as in the i-η experiments the configuration with the TGZO sputtered layer has the lowest electrode polarization followed by CT30 and TGZ100. It is not excluded that at higher temperatures than covered in our experiments the CT30 layer turns out to have the lowest resistance. The bare solid electro-

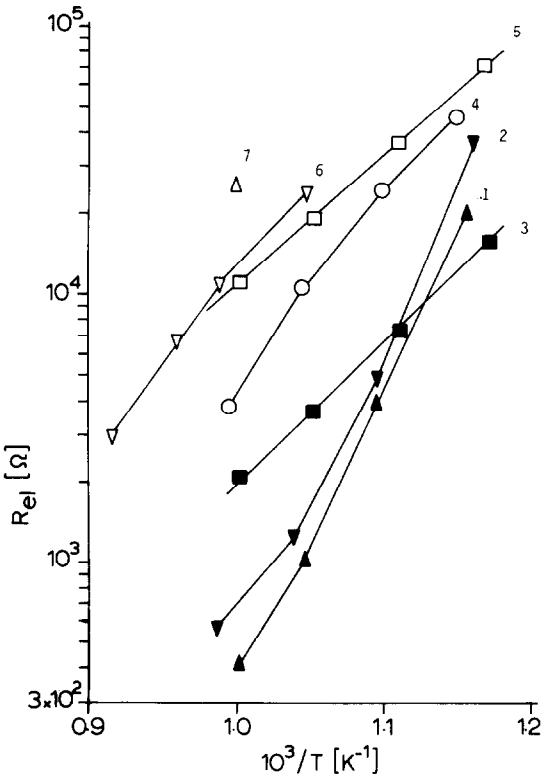

Fig.1. Scaled electrode resistances (R_{el}) as a function of temperature at P_{O_2} = 0.21atm.
1: 600 nm CT30/Pt 2: 600 nm TGZ0/Pt
3: 600 nm TGZ0/Au 4: 600 nm CT30/Au
5: 150 nm TGZ100/Au 6: 150 nm CT30/Au
7: bare TGZ0

lyte shows the highest resistance.

All electrode configurations with the Au-strip show a similar activation enthalpy of about 100 kJ/mol, except for the 150nm and 600nm CT30 layers, where the activation enthalpy increases for higher temperatures. For the 600nm TGZ0 and 150nm CT30 it was found that the activation enthalpies were independent of P_{O_2}. The activation enthalpy for the bare solid electrolyte is somewhat larger.

Evidently the configurations with the Pt-strip perform better in the high temperature range. Towards lower temperatures the curves for Pt and Au approach, which is an interesting point for pumping applications.

For Pt hardly any difference in R_{el} is noticed whether the sputtered layer consists of TGZ0 or CT30. The curves of R_{el} versus T show a similar bend, with a high value of the activation enthalpy at the lower temperatures changing to a lower value at the higher temperatures. This indicates a change in rate determining step, as becomes clear from the P_{O_2} dependence of R_{el}. Apparently the influence of Pt on the electrode reaction process is large and obscures possible influences of the electrolyte surface layer.

TABLE I. Activation enthalpies for R_{el} for the various electrode configurations. In cases where no Arrhenius behaviour was observed for R_{el} the numbers in the column for ΔH describe the gradual transition in the slope of the curves. The first number shows the low temperature limit, the second shows the high temperature limit.

electrode configuration	strip	ΔH (kJ/mol)	P_{O_2} (atm)
bare TGZ0	Au#	120	0.21
600 nm TGZ0	Au	101	0.01
"	Au	106	0.21
"	Au	110	0.43
"	Pt	240-140	0.21
150 nm CT30	Au	100-150	0.21
600 nm CT30	Au	100-150	0.21
"	Pt	240-140	0.21
150 nm TGZ100	Au	99	0.21

For this configuration a symmetrical two electrode cell was used with Au strips to carry out temperature dependent frequency dispersion measurements. Consequently these R_{el} results cannot be compared quantitatively with the other results which were scaled. However it is allowed to compare ΔH values.

Fig. 2 shows the P_{O_2} dependence of R_{el}. It is seen that for all configurations with a Au-strip the lines run parallel. R_{el} varies as $P_{O_2}^m$, with $-0.45 < m < -0.50$ (±0.05 for each line). In the case of the bare solid electrolyte sample m=-0.42(±0.05) and for the Pt-strip on 600 nm CT30, m=-0.34(±0.05). In the latter case m changes to a positive value around $P_{O_2} \approx 0.1$ atm. This was found too by other investigators for Pt-electrodes (e.g. 1,2) and it can be related with the fraction of occupied adsorption sites. At high temperatures $\theta < 1/2$ (θ = fraction of occupied surface sites) and at low temperatures $\theta > 1/2$. The fact that the P_{O_2} value at which the sign of m changes, decreases for decreasing temperature, implies that the activation enthalpy for the electrode reaction (measured at $P_{O_2} \approx 0.1$ atm) in this temperature range

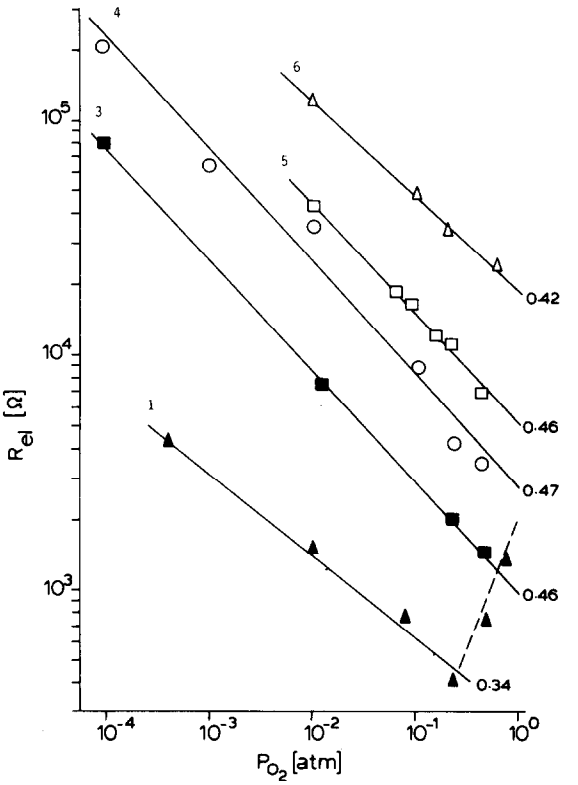

Fig.2. Scaled electrode resistances as a function of P_{O_2} at T ≈ 727°C.
1: 600 nm CT30/Pt 3: 600 nm TGZ0/Au
4: 600 nm CT30/Au 5: 150 nm TGZ100/Au
6: bare TGZ0

covers a change in the mechanism. For the configurations with the Au-strip no such change in sign of m was observed, which implies that θ < 1/2 in the whole P_{O_2} range investigated.

2.2 Capacitive behaviour

Figs.3a-f show the complex impedance diagrams for the various electrode configurations investigated. The inset of most figures shows the high frequency part of the polarization arcs on an enlarged scale. Numbers along the arcs indicate ^{10}log (frequency) values.

The polarization arcs generally consist of a relatively large semicircle towards the lower frequencies. In the case of electrode configurations with a Pt-strip and in the case of the 600 nm sputtered TGZ0 layer with a Au-strip, the semicircles show rather large depression angles (up to 35°) and are sometimes skewed. For the mixed conducting oxides CT30 and TGZ100 sputtered layers with a Au-strip the semicircle depression angles are relatively small (10-15°).

Towards the high frequencies in most cases a straight line behaviour is observed, the behaviour of which is independent of P_{O_2} (inset of the figures). The bare solid electrolyte with the Au strip shows a polarization consisting of two partially separated arcs. The low frequency arc has a rather low semicircle depression angle (≈ 10°).

The impedance data were interpreted in terms of tentative equivalent electrical circuits. Circuit parameters were obtained using a non linear least squares refinement program (3). For simplicity the constant phase element (CPE) is used in the refinement procedures:

$$Y(CPE) = Y_o(j\omega)^n \qquad [1]$$

With n=1 this element represents a capacitance and for n=0 a resistor. For n=0.50 the CPE equals a classical Warburg impedance (2) in a semi-infinite medium:

$$Z(W)=\sqrt{2}K_W(j\omega)^{-1/2} \text{ or } Y(W)=(\sqrt{2}K_W)^{-1}(j\omega)^{1/2} \qquad [2]$$

The Warburg impedance describes a diffusion process and takes a different form for particular boundary conditions (1,4). The complete expression for a R-type Warburg impedance (R-W) is:

$$Y(R\text{-}W) = Y_o(R\text{-}W)\times\beta(1+j)\times\text{cotanh}\,[\beta(1+j)] \qquad [3]$$

where $\beta = \delta\sqrt{\frac{\omega}{2D}}$, $Y_o(R\text{-}W) = \frac{n^2F^2C\,D}{RT\delta}$, δ is a characteristic diffusion distance, C the equilibrium concentration, D the diffusion coefficient and ω the angular frequency 2πf. In the limit $\delta >> \sqrt{\frac{2D}{\omega}}$, i.e. in the case where the diffusion medium can be considered semi- infinite, [3] reduces to [2]. The Warburg constant, consequently, is defined by:

$$K_W = \frac{RT}{n^2F^2C\sqrt{2D}} \qquad [4]$$

The low frequency part of the impedance diagrams is discussed first. Depressed semicircles can be analyzed with a resistance (R) and a CPE in parallel (the depression angle equals $n * \frac{\pi}{2}$). Small semicircle depression is usually attributed to a relaxation process with a spread in relaxation times, for instance described by a Cole-Cole distribution function around $\omega_o = (RC)_{average}$ (5,6). Using the CPE and R parallel circuit, the average value of C is obtained from $(RC)_{average} = (Y_oR)^{1/n}$. This

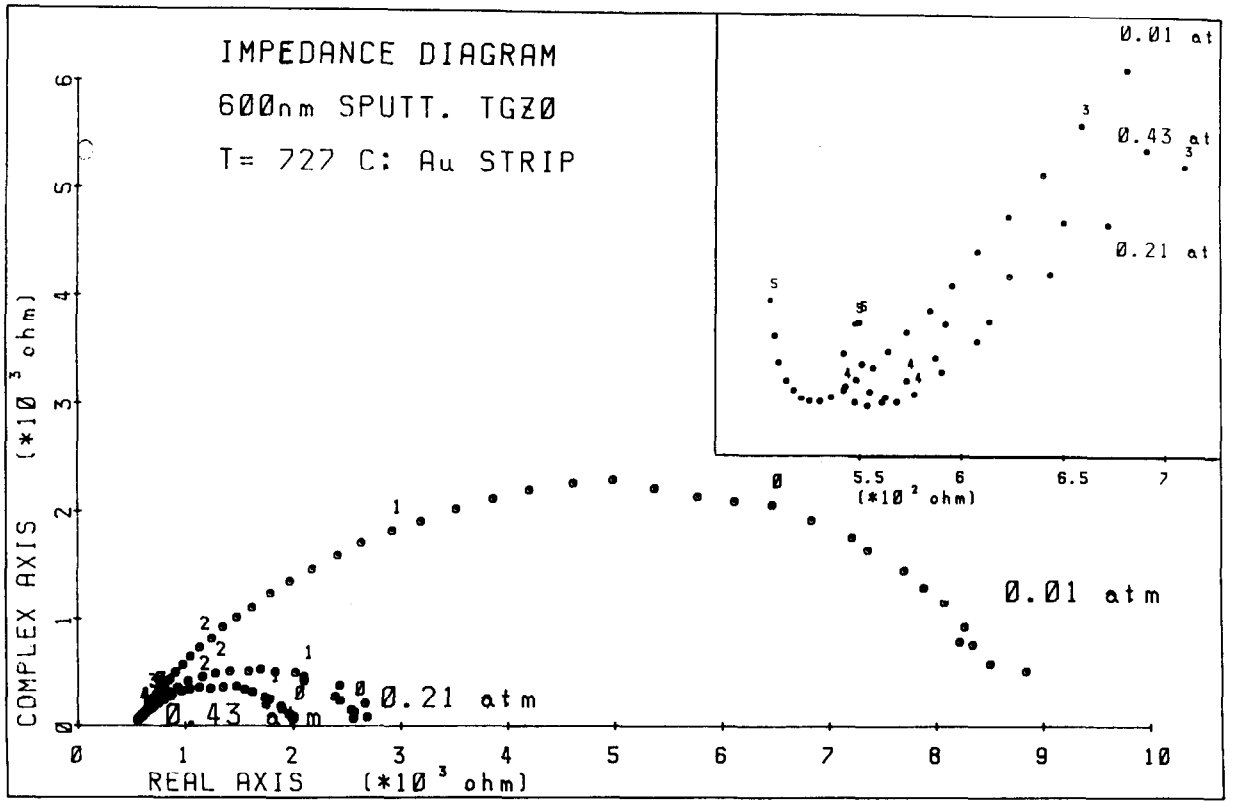

Fig.3a Polarization curves for a 600 nm sputtered layer of TGZO at varying P_{O_2}.

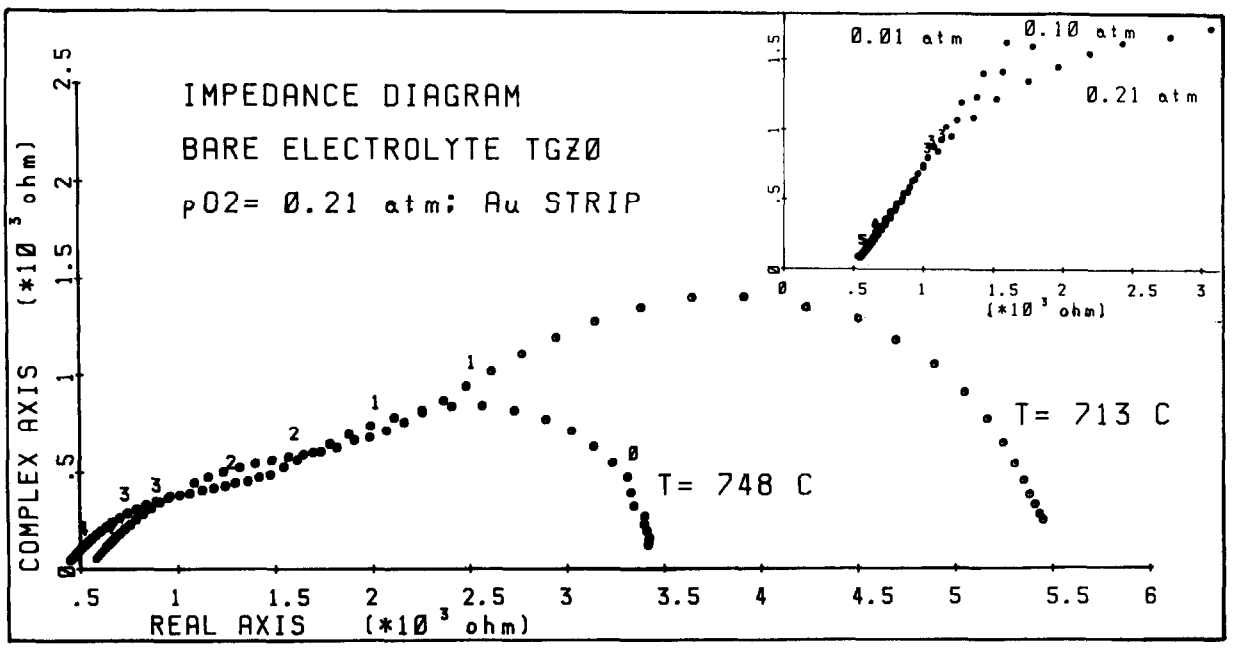

Fig.3b Polarization curves for the bare solid electrolyte sample (see footnote Table I)

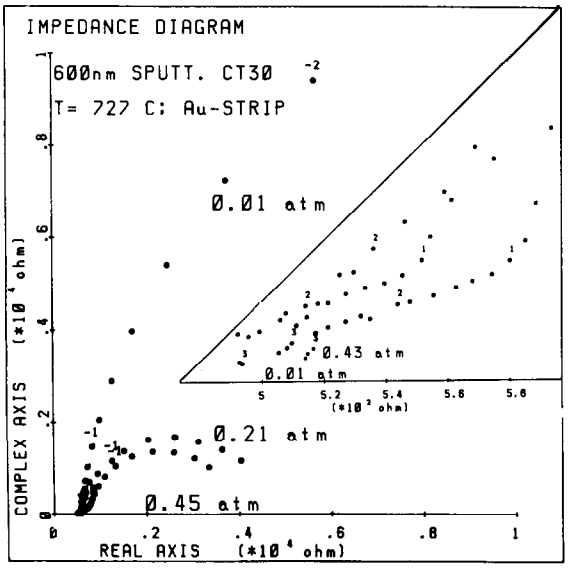

Fig.3c Polarization curves for a 600 nm sputtered layer of CT30.

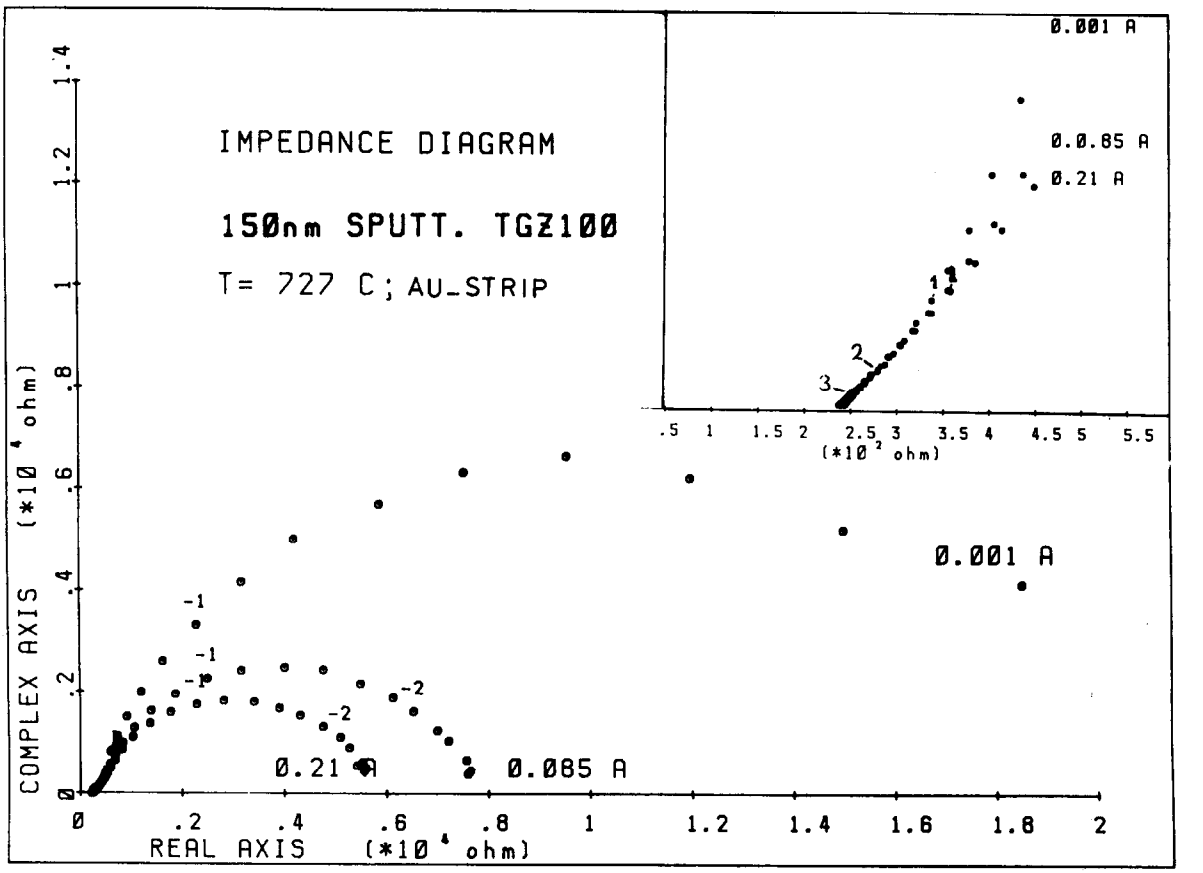

Fig.3d Polarization curves for a 150 nm sputtered layer of TGZ100.

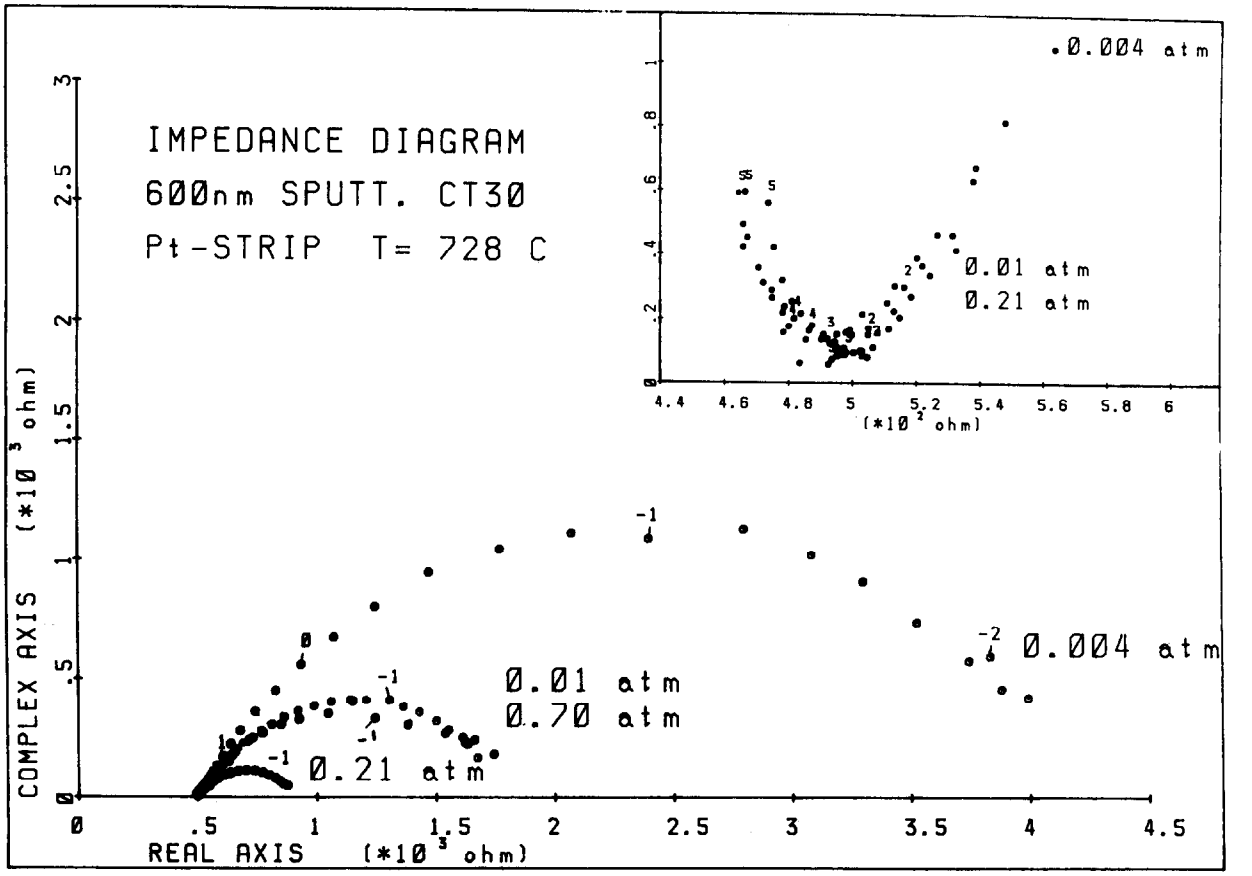

Fig.3e Polarization curves for a 600 nm sputtered layer of CT30 and Pt-strip contacts.

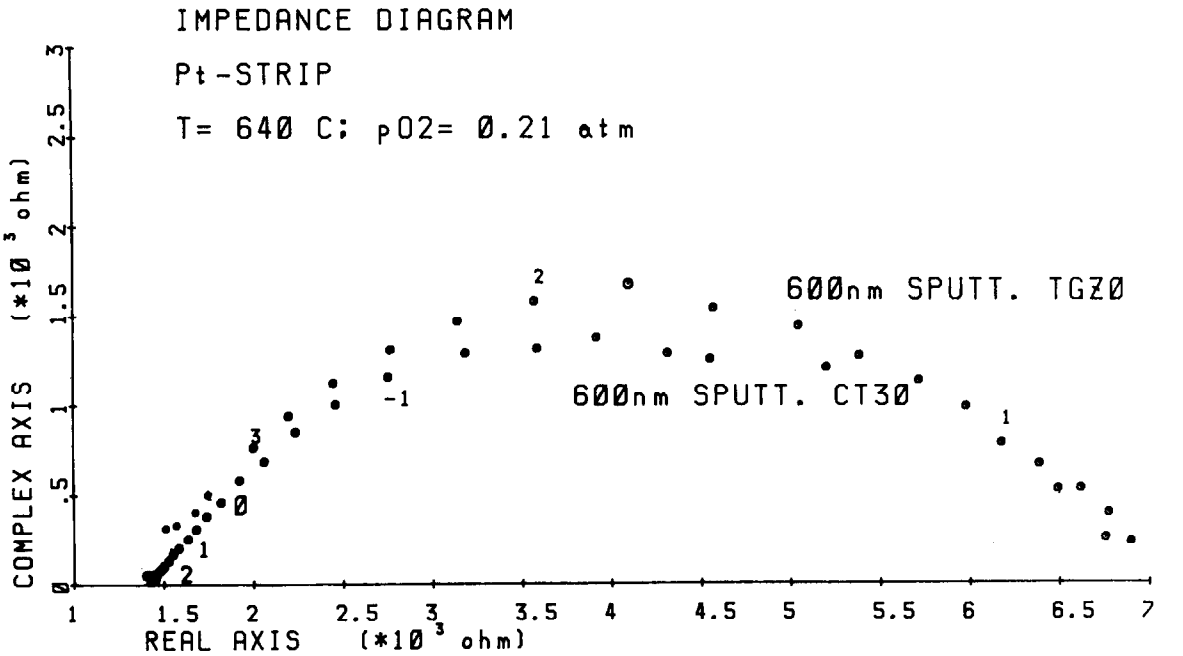

Fig.3f Polarization curves for TGZ0 and CT30 sputtered layers with Pt-strip contacts. Note the different frequency ranges.

TABLE II.
Fitted results for the low frequency part of the impedance diagrams at T = 727°C and P_{O_2} = 0.21 atm (R and CPE in parallel).

Configuration	Strip	R (Ω)	CPE Y_o	n	"C" (F)
bare - TGZO	Au	3.4×10^{4}	1.3×10^{-6}	0.89	8.7×10^{-7}
600 nm TGZO	Au	2.2×10^{3}	1.7×10^{-5}	0.58	1.6×10^{-6}
600 nm CT30	Au	4.1×10^{3}	7.4×10^{-4}	0.90	8.5×10^{-4}
150 nm CT30	Au	1.5×10^{4}	2.0×10^{-4}	0.85	3.8×10^{-4}
150 nm TGZ100	Au	7.3×10^{3}	4.2×10^{-4}	0.87	5.0×10^{-4}
600 nm TGZO	Pt	6.0×10^{2}	6.6×10^{-6}	0.58	1.2×10^{-7}
600 nm CT30	Pt	4.1×10^{2}	9.5×10^{-4}	0.65	5.8×10^{-4}

procedure was followed for the polarization arcs with small semicircle depression angle.

Semicircles with rather large depression angles may result from the contribution of a diffusion process to the electrode reaction(1). For instance a Warburg element (W) in parallel to a resistance results in a semicircle with depression angle 45°. An alternative way of interpreting large depression angles can be effected by using circuits of branched ladder networks. Scheider postulates that the capacitive behaviour of the electrode polarization is totally ascribed to charge spreading in the diffuse double layer and a frequency dependent capacitance resulting from the microscopic surface roughness (7). Such a situation is likely to occur for the noble metal strip-solid electrolyte or sputtered layer contact.

For comparison the capacitive value was also calculated in the case of the impedance diagrams with large semicircle depression angles using the CPE description.

Values of the calculated capacities are given in Table II and Figs. 4 and 5 (scaled values). Obviously large differences are found between the solid electrolyte surfaces of TGZO on the one hand and the mixed conducting surface layers of CT30 and TGZ100 on the other. The type of electrode strip (Pt or Au) has no significant influence on the high C-values determined for CT30 and TGZ100. The C-values for a 150 nm sputtered layer are perhaps somewhat lower than for a 600 nm sputtered layer. The temperature influence seems to be small, but an increasing P_{O_2} leads to higher C-values in case of TGZ100 and CT30 and lower C-values in case of TGZO.

At the high frequency side of the impedance diagrams straight lines are observed in many cases. For the TGZO bare specimen and for the TGZO sputtered layer with the Au strip this line is observed at relatively large frequencies (10^{4}-10^{5} Hz), while for the Tb-containing sputtered layers, both with Au and Pt strips the frequency range is about 10^{3}-10^{1} Hz. This points to considerably larger relaxation times for the predominant process in the case of mixed conducting oxides. It is noticed that

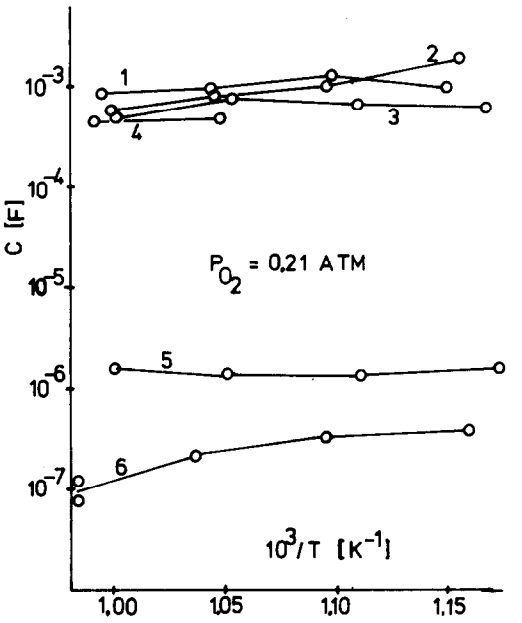

Fig.4. Scaled electrode capacitance as a function of temperature.
1: 600 nm CT30/Au 2: 600 nm CT30/Pt
3: 150 nm TGZ100/Au 4: 150 nm CT30/Au
5: 600 nm TGZO/Au 6: 600 nm TGZO/Pt

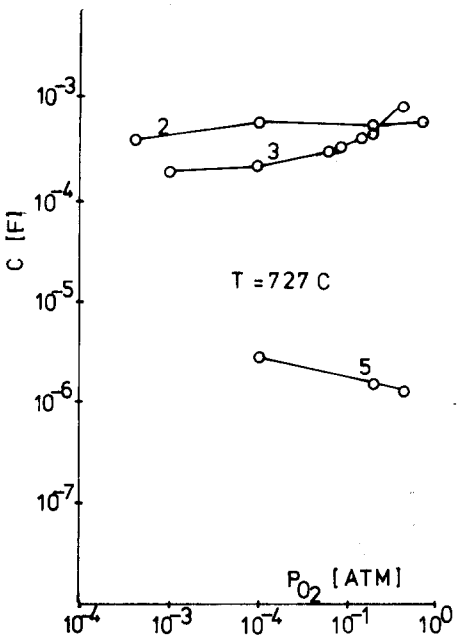

Fig.5. Scaled electrode capacitance as a function of P_{O_2}.
2: 600 nm CT30/Pt 3: 150 nm TGZ100/Au
5: 600 nm TGZ0/Au

this part of the impedance behaviour is independent of P_{O_2}.

From the impedance data for these high frequency ranges Y_o and n can be calculated, using the CPE description. For CT30 and TGZ100 it results that Y_o is thermally activated with $\Delta H \approx 40$ kJ/mol, which is also the value for the activation of K_W, when $n \approx 0.50$.

For the bare TGZ0 specimen two rather separated arcs were observed (Fig. 3b). A complete description in terms of an equivalent circuit involves two parts in series, each part consisting of a CPE and a resistance in parallel. The high frequency part has $n \approx 0.50$ and the low frequency part has $n \approx 0.90$). It is noted that the high frequency part is rather P_{O_2} independent and that K_W^2 (and hence $C^2 \times D$) and the parallel resistance are activated with $\Delta H \approx 90$ kJ/mol, indicative of an electrolyte related process.

3. DISCUSSION.

3.1 Au strip electrodes

All layer electrode configurations with a Au strip showed similar behaviour in the electrode reaction, with respect to the values of m and ΔH at low temperature, while at $T \approx 1000$ K values of $\alpha_a^* \approx \frac{3}{2}$, $\alpha_c^* \approx \frac{1}{2}$ and $m \approx \frac{-1}{2}$ were obtained. This indicates that the reaction mechanism shows similarities for all electrode configurations, irrespective of the presence of mixed conductivity in the surface layer of the electrolyte phase.

In principle both a reaction mechanism with charge transfer being rate determining and one with mass transport limitation can be considered. Considering charge transfer limitation, the fact that α_a^* and α_c^* are not equal indicates asymmetry in the sequence of reaction steps. For a large number of possible mechanisms, concerning both dissociatively and associatively adsorbed oxygen species, and concerning situations in which different numbers of electrons are being transferred at the same time, values of α and m can be predicted (2,8). No consistent mechanism with pure charge transfer being rate determining was found which was able to describe the present results.

Models including diffusion limitation in the rate determining process of the electrode reaction have been studied in the literature too. Wang and Nowick presented a model in which surface diffusion of atomic oxygen on noble metal electrodes was coupled to a charge transfer reaction step(10). The model predicts $\alpha_a^* = \frac{3}{2}$, $\alpha_c^* = \frac{1}{2}$ and $m = \frac{-3}{8}$, if diffusion limitation dominates, while the true Faradaic coefficients ($\alpha_c = \alpha_a = 1$) and $m = \frac{-1}{4}$ are found for charge transfer limitation. This model describes experimental results of these authors for porous Au and Ag, and Pt-foil electrodes on doped ceria solid electrolytes (500-800°C, 10^{-5}-1 atm). We used a modified model of this type.

An analogous model was very recently described by Nguyen et al. (9). These authors, investigating Sc-stabilized zirconia with Au-paste electrodes, showed a model in which surface diffusion of O_2^- species is rate controlling the electrochemical step. It was argued by these authors that adsorption and surface diffusion of oxygen is more likely to occur on the solid electrolyte phase than on the Au particles. The electrochemical reaction sites are connected to regions where the porous Au electrode and the solid electrolyte phase are in contact with each other.

With this model, it was deduced that if diffusion limitation dominates, the apparent charge transfer coefficients ($\alpha_a^* = \frac{3}{2}$ and $\alpha_c^* = \frac{1}{2}$) deviate from the real Faradaic coefficients ($\alpha_a = \alpha_c = 1$) and that $m = \frac{-1}{2}$. On the other hand, if charge transfer limitation dominates, the apparent charge transfer coefficients became equal to the real coefficients

and m = $\frac{-1}{4}$. For almost all their experiments Nguyen et al. found that diffusion limitation dominated with an activation enthalpy of 97 kJ/mol, which agrees very well with values found in our study.

Models of the cited type, which combine diffusion limitation and charge transfer limitation, well explain our experimental results. At the higher temperatures diffusion limitation seems to dominate and the current-overvoltage data can be fitted to $i = i_{o,app}[\exp(\frac{3}{2}\eta^*) - \exp(-\frac{1}{2}\eta^*)]$. Here $i_{o,app}$ is a function of the parameter i_o/Q and Q is a dimensionless parameter that is a measure of the relative ratio of the charge transfer exchange rate and the diffusion rate. Q always includes a characteristic distance along which diffusion takes place (ℓ), and the product of the diffusion coefficient (D) times the concentration of oxygen species at the adsorption site (C_o). In the model presented by Wang and Nowick $Q = (\frac{i_o \ell^2}{2eDC_o})^{1/2}$ (10). At lower temperatures the slight decrease of α_a^* suggests that charge transfer limitation becomes more important.

At $P_{O_2} < 10^{-2}$ atm i-η curves were observed that showed properties characteristic for limiting currents according to eq. [3] and [4] in part I. This confirms that diffusion limitation is at least partially present at higher values of P_{O_2}.

No clear indication of the type of mechanism can be obtained from the value of the activation enthalpy (≈ 100 kJ/mol) since similar values are reported in the literature for both diffusion limited and charge transfer limited processes (1,9,10).

The type of oxide surface layer has a pronounced effect on the relative positions of the i-η curves, as was observed in our experiments. Since values of α_a^* and α_c^* are comparable for the various sputtered oxide layers, the difference in the electrode polarizations can only originate from the fact that both charge transfer and diffusion rates are different to a similar extent. The diffusion flux is determined by the product D × C_o and the effects of D and C_o cannot be separated simply. Thus a TGZO sputtered layer has the best properties for adsorption (C_o) and/or surface diffusion (D), and the TGZO bare solid electrolyte has the worst. Incorporation of Tb or mixed (p-type) conductivity negatively influences the properties of C_o and/or D. These results point to the fact that surface diffusion along the solid electrolyte or sputtered layer phase rather than surface diffusion along the Au-strip contact prevails. This is in agreement with the fact that m ≈ -0.50 was found, in correspondence with the model of Nguyen et al. which assumes solid electrolyte surface diffusion to prevail.(9).

In order to explain why sputterd layers perform better than the bare solid electrolyte sample, it is interesting to refer now to the results of the catalytic CO-oxidation experiments on TGZ powders (11). These results showed that oxides which had been given a heat treatment at 1100-1300°C were most active. This corresponds to the heat treatment at 1100°C given to the freshly sputtered oxide surface layers. On the other hand it was shown in the present study that preferential orientation occurs within the grains of the sputtered layer. The effect of orientation is not known at present, but in analogy to known effects for adsorption processes on metals, it may have a pronounced effect on adsorption in this case.

The differences in electrode performance between the Tb-containing sputtered layers and the TGZO sputtered layer can result from differences in adsorptive capacity too. It was noticed (11,12) that for Tb-containing oxides the reoxidation step in the catalytic oxidation of CO was rate determining. This step involves the uptake of oxygen and the donation of electrons, similar to the cathodic reaction described here. It is suggested that electron donation is hindered by the p-type character of the CT30 and TGZ100 surface layers, in which electron-holes are the mobile charge carriers. Hence it is worth to continue investigations of O_2 redox reactions with n-type mixed conducting oxides too. The stronger decrease of the electrode resistance at higher temperatures for CT30 compared to TGZ100 possibly results from the fact that Ce-containing oxides tend to become n-type semiconductors at higher temperatures, annihilating the p-type behaviour of CT30 due to the presence of Tb.

The above mentioned results do not imply that p-type materials should not be useful in anodic oxidation reactions of other reactants (e.g. CO, methanol, etc.)

3.2 Pt strip electrodes

Irrespective whether a sputtered layer of CT30 or TGZO was applied, the electrode resistance and its temperature dependence for the electrode combinations with a Pt strip are different from the combinations with Au. The similar behaviour of the CT30 and TGZO sputtered layer combinations, in the case of Pt, suggests that the rate determining step in the electrode process is closely related to the properties of the Pt-strip part of the electrode.

The mechanism can be adequately described by assuming that charge transfer limitation and atomic diffusion limitation on the Pt-metal

cooperate. This results from the fact that the values of α_a^*, α_c^* and m correspond with intermediate values as given by Wang and Nowick (10). From our experiments $\alpha_a^* \approx 1.1$, $\alpha_c^* \approx 0.7$ and $m \approx -0.34$ (±0.05), which falls in between the values $\alpha_a = \alpha_c = 1.0$ and $m = -\frac{1}{4}$ for charge transfer limitation and $\alpha_a^* = \frac{3}{2}$, $\alpha_c^* = \frac{1}{2}$ and $m = -\frac{3}{8}$ for diffusion limitation. The impedance diagrams correspond with the polarization behaviour found for Pt gauze electrodes by Verkerk et al. (1).

3.3 Electrode capacitance

It is supposed that the electrode capacitance, presented in Fig.4 and Fig.5, corresponds with the double layer capacitance in the case of the ionic conducting TGZ0 electrode configurations. Taking a mean value of 10^{-6} F and the surface area of the Au and Pt strip ($15mm^2$) the double layer capacitance should equal 7×10^{-2} F/m^2. This is quite a small value compared with literature data ranging from 0.3 - 5 F/m^2 (1,10). Consequently, it is concluded that actually only 2 - 20% of the strip surface is effective in the electrode reaction. It should be remembered that this holds for scaled values of the electrode resistance. A similar conclusion can be drawn from the experiment in which two gold strips were used on both sides of a bare specimen in a two electrode impedance measurement. Now the measured electrolyte resistance can be compared with specific conductivity data for TGZ0 (13) from which an effective contact surface of ≈10% of the geometrical one can be estimated.

Using the value of the geometrical contact surface (15 mm^2) a minimum value of the electrode capacitance of 70 F/m^2 is obtained in the case of CT30 and TGZ100 sputtered surface layers. Using 10% as an average value of effective surface area contact, the capacitance is 700 F/m^2. Clearly this value is too large to result from the double layer capacitance, connected to oxygen vacancy redistribution in the outmost surface layers. The capacitance will rather be a pseudocapacitance, which is frequency dependent.

It is supposed that this very high capacitive contribution results from electronic charge injection at the electrode strip contact, which is not compensated immediately by oxygen transport. Effectively, this implies that the stoichiometry of the mixed conducting oxide layers is changed for very low frequencies. This effect also explains the hysteresis observed in the i-η curves.

The value of C can be related to the number of electron holes present. In (13) it was shown that $[Tb^{4+}]$ and the electronic conductivity decrease in parallel, when the P_{O_2} is decreased. The value of C also decreases for

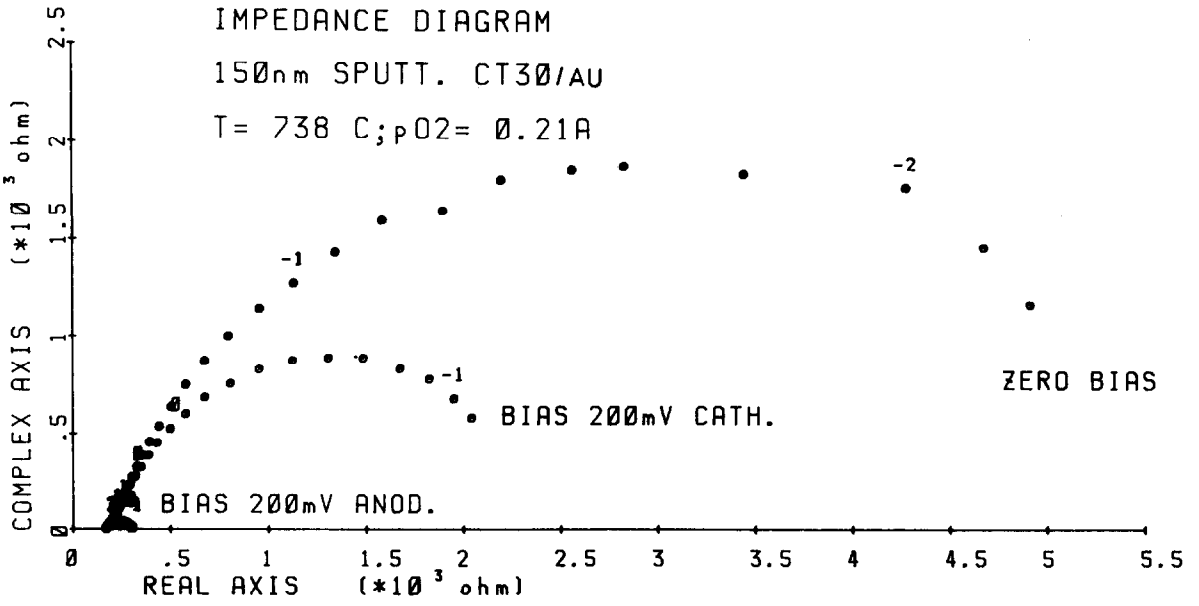

Fig.6. Polarization curves at three different values of bias conditions.

decreasing P_{O_2}. Another illustration of this relation between C and $[Tb^{4+}]$ is seen in the impedance diagrams for measurements under bias conditions, as is shown in Fig.6. The diagrams are dominated by the difference in electrode resistance, corresponding with the Butler-Volmer behaviour, but C-values change too. At a negative potential of 200 mV C = 1.4×10^{-4} F, for zero bias C = 4.4×10^{-4} F and at a positive potential of 200 mV at the working electrode, C = 7.4×10^{-4}F. This variation of C with the potential results from the fact that the stoichiometry of the mixed conducting sputtered layer is changed under bias conditions.

The differences in capacitive behaviour of TGZ0 and CT30 is best illustrated in Fig.3f, which shows the impedance diagrams for a Pt-strip at same T and P_{O_2}. Although the polarization arcs are quite similar (R_{el} values are almost equal), the capacitive values vary over 3 decades, indicated by the numbers along the polarization arcs. The large capacitive values for CT30 and TGZ100 lead to relatively long relaxation times for the electrode reaction. This can be a severe problem in the use of these materials in sensors, which have to show short response times on changing P_{O_2}.

3.4 High frequency electrode polarization

A straight line was observed at the high frequency part of the electrode polarization arcs, which extends over several decades of frequency and the angle of which with the Z'-axis is between 35 and 55°. This implies that a diffusion process is most likely to cause the polarization effect. The fact that the behaviour is P_{O_2} independent suggests that it concerns a bulk diffusion process. In the case of CT30 and TGZ100 both electronic and ionic charges could be responsible for the diffusion process. The activation enthalpy of 35-40kJ/mol for Y_o (and for K_W when n=0.50) can be related to the activation of the product $C_o\sqrt{D}$ from equation [4]. Assuming C_o to be independent of T to first approximation, the diffusion is activated with an activation enthalpy of 70-80 kJ/mol. This value is somewhat higher than that for electronic conductivity (60kJ/mol for TGZ100 and 52 kJ/mol for CT30, chapter VII in [11]) but lower than the values for ionic conductivity (≈125 kJ/mol for TGZ100 and ≈ 115 kJ/mol for CT30). Therefore the diffusion is thought to result from a reorganization of electronic charges within the sputtered layer in a zone adjacent to the interface with the metal, due to the applied AC signal.

In the case of TGZ0 the straight line behaviour was found at higher frequencies and with an activation enthalpy of 90 kJ/mol. Here reorganization of ionic charges (oxygen vacancies) can be considered, since the activation enthalpy for oxygen ion conductivity in TGZ0 is in the same order. Further experiments are needed to elucidate the actual diffusion mechanism.

4. CONCLUSIONS

1. Results of complex impedance analysis for small signal frequency dispersion experiments on the electrochemical oxygen gas reaction show the same trends in the polarization behaviour as was concluded from current-overvoltage experiments (see part I). Sputtered layers on top of a solid electrolyte phase improve the oxygen electrode reaction compared to a bare specimen. The largest improvement is found for the ionic conductor TGZ0, and lesser improvements for the p-type mixed conductors CT30 and TGZ100.
2. High electrode capacitances were found in the case of mixed conducting surface layers. The minimum value of the specific capacitance is 700 F/m^2, taken into account the fact that about 10% of the geometrical strip surface is in contact with the oxide surface. This C-value is larger than values usually found for double layer capacitances and points to pseudo-capacitances, arising from injection of electronic charges in the mixed conducting surface layer. Because of these high C-values large electrode relaxation times are found, which implies long response times in sensor applications.
3. i-η curves follow a Butler-Volmer type of equation. Experimental values of i_o and α are changed from their true Faradaic values by diffusion phenomena. Most probably a diffusion process is rate controlling the charge transfer process. Surface diffusion along the solid electrolyte or sputtered layer phase can explain the difference in experimental results for different materials.

5. ACKNOWLEDGEMENT

Mr. H. Kruidhof and Mr. B. van Dongen are acknowledged for their experimental assistance. This investigation was supported by the Netherlands Foundation for Chemical Research (SON) with the financial aid from the Netherlands Organization for the Advancement of Pure Research (ZWO).

6. REFERENCES

(1) M.J. Verkerk, M.W.J. Hammink, A.J. Burggraaf, J.Electrochem.Soc. 130 (1983) 70 and M.J. Verkerk, A.J. Burggraaf, ibidem 130 (1983) 78.

(2) A.J.A. Winnubst, A.H.A. Scharenborg, A.J. Burggraaf, Solid State Ionics 14 (1984) 319.

(3) B.A. Boukamp, accepted for publication in Solid State Ionics.

(4) G.H.J. Broers, M. Schenke, Proc.Int.Conf. on Fuel Cells, (Akademie Verlag, Dresden, 1967), p.299.
H.T. Cahen, Ph.D. Thesis, State University Utrecht, The Netherlands (1980).

(5) M. Kleitz, J.H. Kennedy, in Fast Ion Transport in Solids ed. Vashishta, Mundy, Shenoy (Elsevier, North Holland, 1979) p.185.

(6) H.J de Bruin and A.D. Franklin, J.Electroanal.Chem. 118 (1981) 405.

(7) W. Scheider J.Phys.Chem. 79 (1975) 2.

(8) H. Okamoto, G. Kawamura, T. Kudo, Electrochimica Acta 28 (1983) 379.

(9) B.C. Nguyen, D.M. Mason, L.M.Rincon-Rubio, submitted to J.Electrochem.Soc.

(10) D.Y. Wang, A.S. Nowick, J.Electrochem.Soc. 126 (1979) 1155, ibidem 126 (1979) 1166 and 128 (1981) 55.

(11) M.P. van Dijk, Ph.D. Thesis, Twente University of Technology, Enschede, The Netherlands (1985).

(12) J.H.H. ter Maat, M.P. van Dijk, G.Roelofs, H. Bosch, G.M.H. van der Velde, P.J. Gellings and A.J. Burggraaf, Mat.Res. Bull. 19 (1984) 1271

(13) M.P. van Dijk, K.J. de Vries and A.J. Burggraaf, Solid State Ionics 16 (1985) 211.